

# The Impact of Including Carbonyl Iron Particles on the Melt Electrowriting Process

Juliane C. Kade, Ezgi Bakirci, Biranche Tandon, Danila Gorgol, Miroslav Mrlik, Robert Luxenhofer,\* and Paul D. Dalton\*

Melt electrowriting, a high-resolution additive manufacturing technique, is used in this study to process a magnetic polymer-based blend for the first time. Carbonyl iron (CI) particles homogeneously distribute into poly(vinylidene fluoride) (PVDF) melts to result in well-defined, highly porous structures or scaffolds comprised of fibers ranging from 30 to 50  $\mu\text{m}$  in diameter. This study observes that CI particle incorporation is possible up to 30 wt% without nozzle clogging, albeit that the highest concentration results in heterogeneous fiber morphologies. In contrast, the direct writing of homogeneous PVDF fibers with up to 15 wt% CI is possible. The fibers can be readily displaced using magnets at concentrations of 1 wt% and above. Combined with good viability of L929 CC1 cells using Live/Dead imaging on scaffolds for all CI concentrations indicates that these formulations have potential for the usage in stimuli-responsive applications such as 4D printing.

## 1. Introduction

Blends of poly(vinylidene fluoride) (PVDF) and magnetic particles, to induce advantageous properties in addition to PVDF's piezoelectricity, are gaining attention<sup>[1–5]</sup> and are being studied for stimulation of cells.<sup>[6]</sup> Different processing techniques for electroactive polymers have been studied;<sup>[7]</sup> however, many require volatile solvents or lack control over the design and/or the resolution. Using melt electrowriting (MEW) to fabricate 3D constructs offers the possibility to process highly porous and well-defined structures without the addition of toxic solvents.<sup>[8]</sup>

MEW is a high-resolution additive manufacturing technique based on an electrohydrodynamic effect to place fibers layer-by-layer to produce designs onto a computer-aided moveable collector.<sup>[9,10]</sup> Briefly, an

applied (air) pressure extrudes the polymer melt out of a metal nozzle, which falls onto the collector substrate to establish a fluid column, or jet.<sup>[11]</sup> With the jet connecting the nozzle and the collector the application of a voltage stabilizes this column so that it can be direct written onto the collector, typically producing uniform fibers with diameters between 5 and 50  $\mu\text{m}$  depending on the polymer and conditions.<sup>[11]</sup> Therefore, MEW bridges the gap between solution electrospun fibers, with diameters commonly in the nanometer range, and extrusion-based printed constructs with an upper resolution limit of  $\approx 100\text{--}150\ \mu\text{m}$ .<sup>[12–14]</sup> The resulting MEW-processed scaffolds are often used to guide cell growth in tissue engineering applications<sup>[15,16]</sup> or to reinforce hydrogels providing mechanical stability and improved handling.<sup>[12,17]</sup>

After poly( $\epsilon$ -caprolactone) (PCL), PVDF is the most commonly MEW-processed polymer<sup>[18,19]</sup> but has not yet been combined with filler particles. While particles of hydroxyapatite (HAp),<sup>[20]</sup> strontium-substituted bioactive glass (SrBG),<sup>[21]</sup> bioactive milk proteins, lactoferrin, whey protein,<sup>[22]</sup> or reduced graphene oxide (rGO)<sup>[23]</sup> have been combined with PCL, particles with magnetic capacity such as carbonyl iron (CI) have not previously been studied for MEW. The CI particles constitute a magnetic powder known for its high thermal stability, cytotoxicity<sup>[24,25]</sup> and are often used in magnetic polymer-based blends.<sup>[5,26,27]</sup> In addition, high particle contents are expected to change the polymer properties and therefore, might require high pressures, to extrude the material, which are not achievable by pneumatically driven MEW printers, or lead to nozzle clogging.


J. C. Kade, E. Bakirci, B. Tandon, P. D. Dalton  
 Department of Functional Materials in Medicine and Dentistry and  
 Bavarian Polymer Institute  
 University Hospital Würzburg  
 Pleicherwall 2, 97070 Würzburg, Germany  
 E-mail: pdalton@uoregon.edu

J. C. Kade, M. Mrlik, R. Luxenhofer  
 Polymer Functional Materials  
 Chair for Advanced Materials Synthesis  
 Department of Chemistry and Pharmacy  
 Julius-Maximilians-University Würzburg  
 97070 Würzburg, Germany  
 E-mail: robert.luxenhofer@helsinki.fi

B. Tandon, P. D. Dalton  
 Phil and Penny Knight Campus for Accelerating Scientific Impact  
 University of Oregon  
 1505 Franklin Boulevard, Eugene, OR 97403, USA

D. Gorgol, M. Mrlik  
 Centre of Polymer Systems  
 Tomas Bata University in Zlin  
 Trida T. Bati 5678, Zlin 760 01, Czech Republic

R. Luxenhofer  
 Soft Matter Chemistry  
 Department Chemistry, and Helsinki Institute of Sustainability Science  
 Faculty of Science, University of Helsinki  
 PB55, Helsinki 00014, Finland

 The ORCID identification number(s) for the author(s) of this article can be found under <https://doi.org/10.1002/mame.202200478>

© 2022 The Authors. Macromolecular Materials and Engineering published by Wiley-VCH GmbH. This is an open access article under the terms of the Creative Commons Attribution License, which permits use, distribution and reproduction in any medium, provided the original work is properly cited.

DOI: 10.1002/mame.202200478

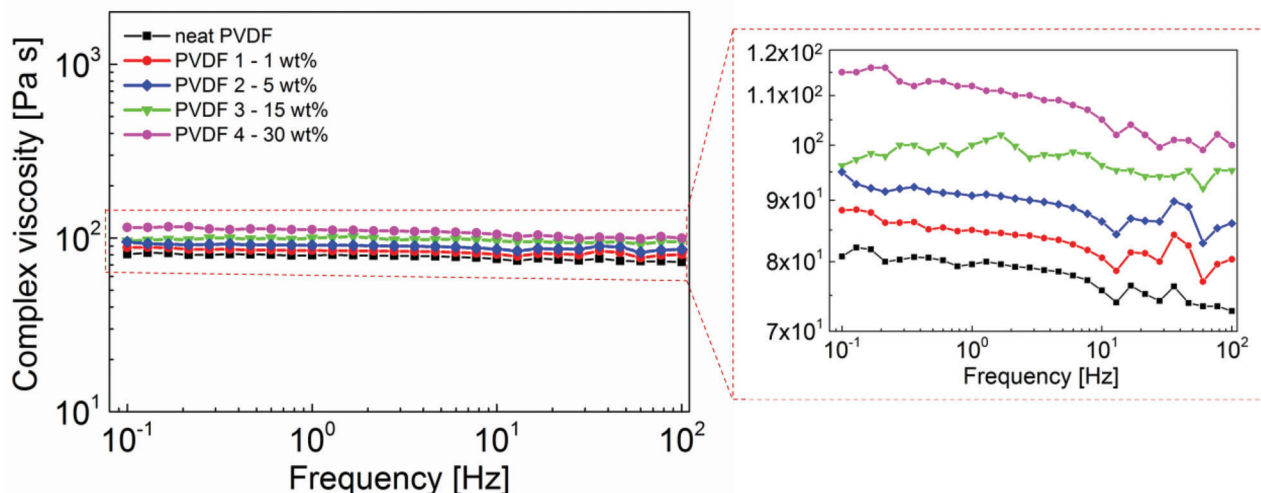


**Figure 1.** Dependence of the complex viscosity on the frequency for various master batches containing different amounts of carbonyl iron (CI) (1–30 wt%) at temperature of 200 °C with the inset showing a magnified view.

Shape changing scaffolds, either induced by different printing parameters<sup>[28]</sup> or through a multiphasic material combination,<sup>[29,30]</sup> are of interest due to their ability to change their configuration.<sup>[31,32]</sup> An interesting class of materials enabling these properties are, for example, hydrogels<sup>[28–33]</sup> and electroactive materials.<sup>[34]</sup> Therefore, 4D printing enables motions or functions of 3D-printed constructs controlled by external stimuli.<sup>[32]</sup> One example of such stimuli responsive materials are magnetically responsive polymers.<sup>[35–37]</sup>

In this study, PVDF blends containing up to 30 wt% CI particles were prepared and characterized for thermal properties and melt viscosity. Different blends with particles showed sufficient MEW processability without nozzle clogging or the need for solvents to lower the viscosity.<sup>[21]</sup> MEW-processed constructs were imaged and characterized using scanning electron microscopy (SEM) and energy-dispersive X-ray spectroscopy (EDX). The magnetic behavior of the printed constructs was shown, cell viability was investigated using L929 CC1 cells over a period of 4 d. Therefore, PVDF containing up to 30 wt% CI particles offers the potential to be used for magnetoactive cell stimulation in tissue engineering.

## 2. Experimental Section

### 2.1. Materials

CI magnetic particles (BASF, Germany) with 99.5% purity, magnetic saturation of 229 emu g<sup>-1</sup> and negligible magnetization saturation,<sup>[24]</sup> were used as received. These particles were also used due to their known cytocompatibility.<sup>[24,25]</sup> PVDF (Sigma Aldrich, USA) formed the polymer matrix of the blends and was used as received. PVDF has  $M_n = 107 \text{ kg mol}^{-1}$ , with a dispersity of  $\mathcal{D} = 2.33$  and was supplied in the form of pellets.

### 2.2. Mixing and Viscosity

The master batches consisting of PVDF and various amount of CI particles (1, 5, 15, and 30 wt%) were mixed using lab-

oratory twin-screw mixing machine DSM MC-15 (Xplore Instruments, Netherlands), where temperature during mixing was set to 200 °C and screw rotation to 50 rpm. The rheological characteristics of the blends were measured utilizing rheometer Physica (MCR502, Anton Paar, Austria) connected to Peltier heating/cooling fixture and parallel-plate geometry (PP10). Samples in form of discs were prepared from the master batches using hot-pressing at 200 °C for 5 min within special molds. The final shape of the samples has a thickness of 1 mm and a diameter of 10 mm. To avoid sample slippage, a constant 0.3 N force was applied to initially determine the linear viscoelastic region (Figure S1, Supporting Information). All further measurements were performed within this region. Subsequently, a frequency sweep in the range from 10<sup>-1</sup> to 10<sup>1</sup> Hz was performed. The values given in the figures are average values obtained from three individual measurements. It should be noted that standard deviation of the individual measurements is smaller than the height of the symbol presented in the **Figure 1**.

### 2.3. Differential Scanning Calorimetry (DSC)

DSC measurements were performed using differential scanning calorimeter (DSC-1, Mettler-Toledo, Switzerland). The nitrogen gas flow rate was set to 20 mL min<sup>-1</sup> and the weight of the investigated samples ranged from 4 to 5 mg. DSC curves were obtained by heating/cooling from -80 to 200 °C and back at a rate of 10 °C min<sup>-1</sup>. All experiments were performed three times, and average values were used. In order to show if the presence of CI particles affects the crystallinity,  $X_c$  of the PVDF based samples was calculated using Equation (1),<sup>[38,39]</sup> where  $\Delta H_m$  is the heat of fusion for individual samples and  $\Delta H_m^0$  is the heat of fusion obtained for 100% crystalline PVDF (104.5 J g<sup>-1</sup>)<sup>[38,39]</sup>

$$X_c = \frac{\Delta H_m}{\Delta H_m^0} \times 100 \quad (1)$$

## 2.4. Melt Electrowriting Printer Configuration

MEW was conducted using a custom-built printer as previously described.<sup>[9]</sup> The material was placed in a glass syringe (3 mL FORTUNA OPTIMA Luer Lock Tip, Poulten & Graf GmbH, Wertheim, Germany) and connected to a metal nozzle (26-gauge with Luer Lock, Carl Roth, Germany), cut to a length of  $7.0 \pm 0.4$  mm. The print head and the nozzle were heated to  $200$  °C for each material with two separate electrical heaters and a controllable air pressure system set to 3 bar enabling extrusion of the melt. Printing parameters were chosen to be constant for the neat PVDF and all blends to be able to compare the resulting samples and to study the influence of the particle content on MEW processability. Moving of the print head in Z-direction and the collector in X- and Y-direction is enabled by linear stages (Bosch Rexroth AG, Lohr am Main, Germany) and controlled via G-code using the software Indra Works Operation (Bosch Rexroth AG, Lohr am Main, Germany). The collector distance to the print head was set to 2.5 mm, a voltage of +1.5 and -1.5 kV was applied to the nozzle tip and the collector, respectively, supplied by a high voltage laboratory power supply (Heinzinger LNC 10000-5 pos/neg, Rosenheim, Germany).

Single layered fibers were printed for fiber diameter analysis onto glass microscope slides (ground edge, cat. No. 631-1552, VWR, Germany). In addition to single fibers, MEW scaffolds were direct-written upon glass microscope slides with  $20 \times 20$  mm in dimensions and fiber orientation of  $0^\circ$ - $90^\circ$  between each alternating layer within the programmed G-code.

## 2.5. Sample Imaging and Videography

For sample imaging, a SEM (Crossbeam 340 SEM equipped with GEMINI e-Beam column, Carl Zeiss Microscopy, Göttingen, Germany) was used. EDX was conducted on 4 nm platinum sputter-coated (Leica EM ACE600, Wetzlar, Germany) blends.

Magnetic behaviour was demonstrated on highly porous structure using PVDF scaffolds containing 30 wt% CI particles and a PVDF scaffold without particles as a non-magnetic control using a magnet. The magnetic properties of the CI particles were investigated using vibration sample magnetometry (VSM) in previous studies.<sup>[24,25]</sup>

Videography was performed using a Nikon Z6 digital camera with Nikon ED 200 mm lens. Editing of the videos was performed using the software DaVinci Resolve 16.

## 2.6. Magnetic Field Measurements

In order to investigate the capability to stimulate fabricated scaffolds, the typical electromagnet utilizing DC magnetic field connected to the DC voltage source Keithley 2401 (Keithley, USA) operating at 24.6 V during measurements provided magnetic field in the range from 40 to 240 kA m<sup>-1</sup> depending on the distance from the electromagnet. The magnetic field strength was checked using TeslaMeter FH-51 with probe HS-TB51 (Magnet-Physik, Germany).

MEW-processed scaffolds were fixed and placed between the electromagnet and a magnetic field of 240, 220, 136, and 64 kA

**Table 1.** Summarized results obtained for various master batches of PVDF containing CI particles up to 30 wt%.

Sample code	$T_m$ [°C]	$\Delta H_m$ [J g <sup>-1</sup> ]	$T_c$ [°C]	$X_c$ [%]
Neat PVDF	$172 \pm 0.8$	$43 \pm 0.2$	$132 \pm 0.2$	$41 \pm 0.6$
PVDF 1-1 wt%	$172 \pm 0.6$	$42 \pm 0.6$	$136 \pm 1.2$	$41 \pm 0.3$
PVDF 2-5 wt%	$172 \pm 0.9$	$41 \pm 0.5$	$137 \pm 0.9$	$39 \pm 0.7$
PVDF 3-15 wt%	$172 \pm 0.2$	$36 \pm 1.3$	$137 \pm 0.7$	$35 \pm 0.4$
PVDF 4-30 wt%	$172 \pm 0.4$	$32 \pm 0.9$	$137 \pm 1.4$	$31 \pm 1.1$

were applied to stimulate the PVDF scaffolds containing 1, 5, 15, or 30 wt% CI particles, respectively.

## 2.7. Cell Adhesion/Viability Tests

The viability of murine fibroblast cell line L929 CC1 (ATCC, Rockville, USA), which were cultured on neat PVDF and PVDF containing 1, 5, 15, and 30 wt% of CI particles scaffolds, were observed via live/dead-staining (LIVE/DEAD Viability/Cytotoxicity Kit, ThermoFisher Scientific). L929 CC1 ( $0.5 \times 10^6$ ) were seeded on each scaffold. Cells were cultured up to 4 d in Dulbecco's Modified Eagle Medium (DMEM) F-12 (+1 vol% Pen/Strep and +10 vol% FCS) (Gibco, Thermo Fisher Scientific Inc., Waltham, MA) at 37 °C (5% CO<sub>2</sub>/95% air). Live/dead-staining was performed and the cell seeded scaffolds were imaged using fluorescence microscopy (Axio Observer, Zeiss equipped with epi fluorescence optics, an MRm camera, and an Apotome; Zeiss, Oberkochen, Germany) with at least three samples for each condition and five different images per sample.

## 3. Results and Discussion

In this study, the processability and the influence on the MEW process of PVDF/CI particle blends were investigated for particle contents ranging from 1 to 30 wt%. Due to long heating times of several hours, both, the thermal stability and the melting temperature of the processed materials are of importance for the MEW process, as slight changes can influence the process.<sup>[40]</sup> Therefore, thermogravimetric analysis (TGA) measurements were conducted and revealed appropriate thermal stability of the neat PVDF, as well as the blends with varying CI particle contents up to 350 °C (Figure S2, Supporting Information). Using DSC, the influence of the particle concentration on the melting temperature was investigated which demonstrated that the melting point of PVDF does not shift by the addition of CI, as it remained at 172 °C despite the increasing amount of the magnetic particles (Table 1 and Figure S3, Supporting Information).

Neat PVDF showed an X-ray diffraction pattern in good accordance with the literature.<sup>[41]</sup> The overall crystallinity was nearly identical for individual master batches shown by the XRD measurements (Figure S3C, Supporting Information), as well as the resulting  $\beta$ -phase contents of the MEW-processed scaffolds calculated from the Fourier-transform infrared spectroscopy (FTIR) analysis (Figure S4, Supporting Information). Similar results have been previously observed in literature for PVDF films containing 1 to 10 wt% CI particles.<sup>[5]</sup> The continual decrease of

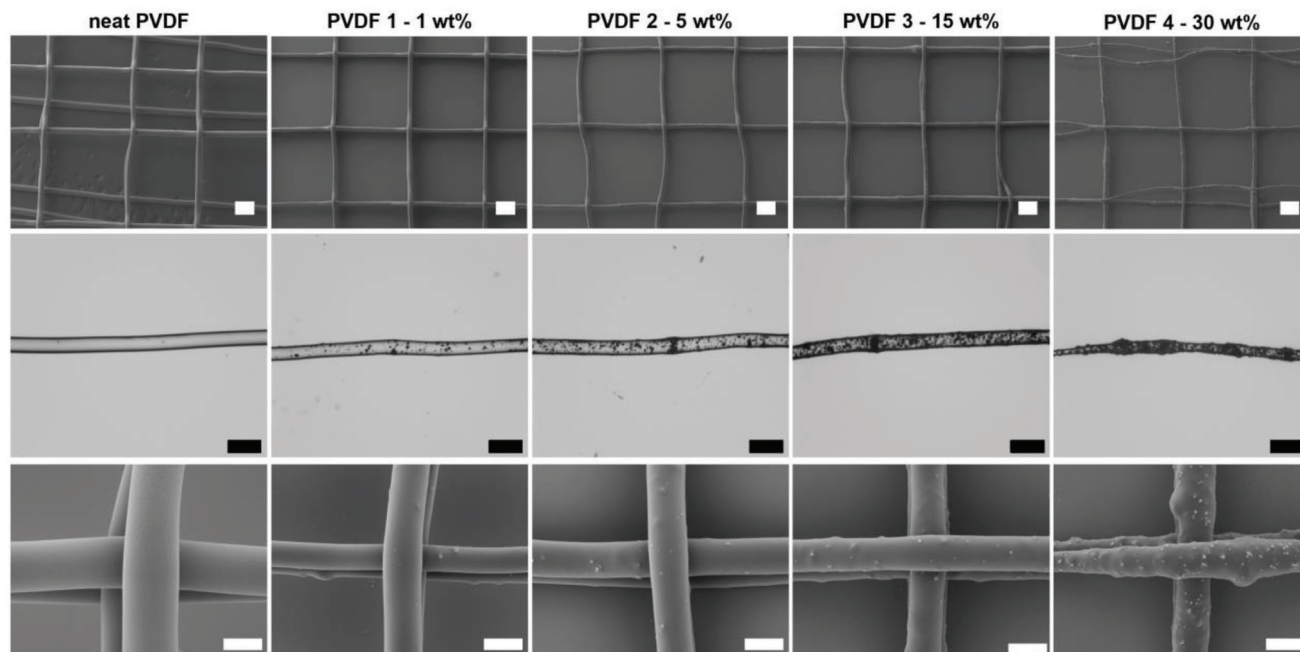


**Figure 2.** Overview SEM images of the scaffolds (top row, scale bar = 250  $\mu\text{m}$ ), and stereomicroscopic (middle row, scale bar = 100  $\mu\text{m}$ ), as well as SEM (bottom row, scale bar = 50  $\mu\text{m}$ ) images of the neat PVDF and blends with increasing magnetic CI particle content.

the crystallinity ( $X_c$ ) was connected to the increasing amount of the magnetic particles in the master batches and thus the lower amount of PVDF present in the system (Table 1).

Another important factor for MEW is the melt viscosity of the polymer. Florczak et al.<sup>[18]</sup> showed that PVDF, investigated under steady shear conditions, has a strong pseudoplastic character and a viscosity around 100 Pa s for low shear rates at 190 °C. In the present study, a different grade of PVDF was employed, and the addition of CI particles could be expected to increase the viscosity. At 200 °C, the viscosity of the blends increases moderately but noticeably in the range from around 70 to 120 Pa s with increasing CI particle content (Figure 1). However, these changes should not significantly impact the ability to perform MEW.

MEW of PVDF and its copolymers, as already shown by Florczak et al.<sup>[18]</sup> and Kade et al.<sup>[42]</sup> provides an option for solvent-free fabrication of well-defined structures using electroactive polymers. Furthermore, combining these materials with magnetic particles offers the possibility to introduce magnetoactivity. Previously, the highest particle content which has been added to a polymer matrix for electrohydrodynamic jetting was 33 wt% of strontium-substituted bioactive glass embedded within PCL.<sup>[21]</sup> However, direct writing of these composite formulations was only achieved using an evaporable solvent to reduce the viscosity.<sup>[21]</sup> The highest particle concentration reported for MEW to date is 7 wt% of hydroxyapatite particles.<sup>[20]</sup>

PVDF could be MEW processed here with different amounts of CI particles (1, 5, 15, and 30 wt%) using MEW without clogging the nozzle and without any further additives or solvents. Interestingly, the printing of all five materials below the critical translation speed (CTS) resulted in fiber pulsing and therefore, major variations of the fiber diameter (Video S1, Supporting Information). Increasing the speed reduced this fiber pulsing

phenomenon. As previously described when MEW-processing PVDF<sup>[18,19]</sup> and its copolymer,<sup>[42]</sup> the rapid solidification of these materials during the printing process can lead to limited adherence onto the collector, as well as reduced fiber stacking and warping of the printed constructs.

In this study, the extruded material cooled down “in air” while the fibers were coiling for printing speeds below the CTS (Video S1, Supporting Information). To direct-write straight fibers of all materials studied in this work, printing speeds of 2000 and 2800  $\text{mm min}^{-1}$  were used. Furthermore, other processing parameters, e.g., collector-to-print head distance, applied voltage, and temperatures, were chosen to result in a stable and homogeneous MEW jet and the parameters were kept constant for the neat PVDF and all blends to enable better comparison and investigation of the particle content onto the MEW process.

Stereomicroscopic images of all processed blends visualize the increasing amount of particles and the color changes to more black fibers depending on the particle content (Figure 2).

When direct writing at speeds greater than the CTS, the neat PVDF fibers showed a homogenous and smooth fiber surface with similar results for the blends containing 1 and 5 wt% of CI particles, as indicated by SEM images (Figure 2). Only for the collector speed of 2000  $\text{mm min}^{-1}$  the neat PVDF resulted in larger fiber diameters and with less accurate fiber placement compared to the blends processed at the same collector speed, which could be improved when adjusting the processing parameter, such as applied voltage, collector speed, and pressure, individually for each direct-written material. Fiber uniformity started to be affected for the PVDF/15 wt% CI, which can also be seen in the higher standard deviation for the fiber diameters (Table 2). The blend containing 30 wt% CI particles resulted in the smallest fiber diameters with nonuniform shape due to the high



**Table 2.** Influence of two different collector speeds on the fiber diameter for neat PVDF and the different PVDF blends containing 1, 5, 15, and 30 wt% CI particles.

Collector speed	Neat PVDF	PVDF 1-1 wt% CI	PVDF 2-5 wt% CI	PVDF 3-15 wt% CI	PVDF 4-30 wt% CI
[mm min <sup>-1</sup> ]	Diameter [μm]				
2000	51 ± 7	42 ± 5	42 ± 5	50 ± 9	37 ± 12
2800	42 ± 9	40 ± 6	43 ± 10	45 ± 12	33 ± 11

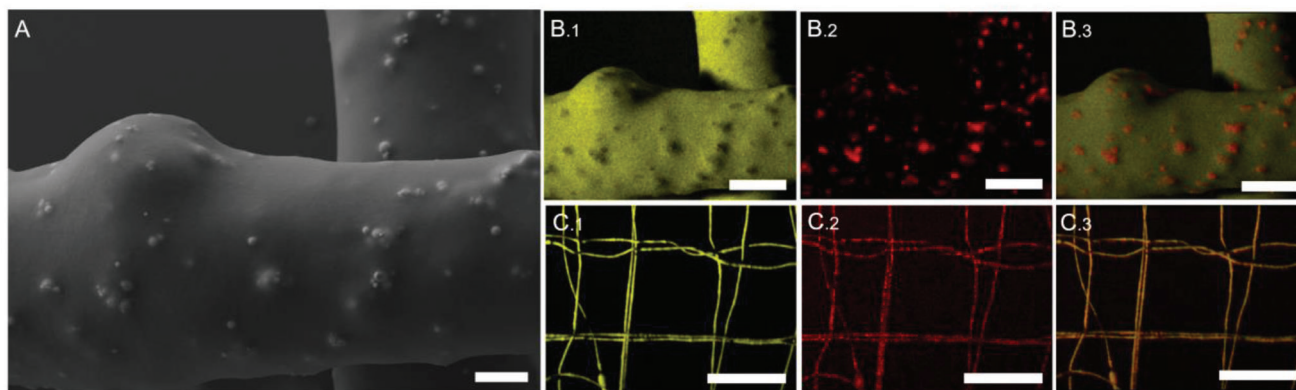


**Figure 3.** A) SEM and B,C) EDX images of a scaffolds printed with PVDF including 30 wt% CI particles showing homogenous distribution throughout the printed fibers. In (B1) and (C1) the fluorine (F) within the PVDF in yellow; in (B2) and (C2) the iron (Fe) in red and (B3) and (C3) the merged images are visualized. Scale bars are A) 10 μm, B) 25 μm, and C) 1 mm.

particle content, however, was still processable without nozzle clogging.

Furthermore, the fiber diameter tested at two different speeds well above the CTS remained similar for the different blends except PVDF/30 wt% CI, which resulted in a decrease of fiber diameters of around 10 μm (Table 2). In addition, the warping of printed constructs was visible for all materials (Video S1, Supporting Information) affecting the printing process and resulting in limited layer stacking, as previously mentioned and observed for PVDF.<sup>[18,19]</sup>

With increasing amount of particles, more particles were visible on the fiber morphology as shown in Figure 2. Even though the particles appeared mostly homogeneously dispersed within the PVDF matrix, the blends with 5 wt% or more CI also showed domains with agglomerated particles. A similar surface morphology was observed in films of 1–10 wt% CI particles in PVDF by SEM showing a rougher surface with increasing particle content compared to neat PVDF films.<sup>[5]</sup>

EDX results of the fabricated scaffolds confirmed the presence of the iron (Fe) and gave further evidence of the rather homogeneous distribution of the particles within the fibers even for PVDF with 30 wt% magnetic particles (Figure 3). In Figure 3A, agglomerations of a few particles were visible on the fiber surface. Similar surface morphologies and particle clusters could be seen previously for PVDF films with different CI particle contents.<sup>[5]</sup> Interestingly, the larger inhomogeneities (bulges) within the fibers were not directly connected to the localised aggregation of CI particles, as these bulges did not show a visible increase or clustering of Fe in EDX (Figure 3B1-3). Similar bulges have been observed

for CI particles (5%–13% (m/m)) dispersed in a polysulfone polymer solution within electrospun fibers, especially with increasing additive content.<sup>[43]</sup> Higher particle amounts within the polymer solution did not enable sufficient fiber production resulting in nozzle clogging due to the high viscosity and density of the incorporated particles.<sup>[43]</sup> Figure 3C1–3 highlights the reduced stacking accuracy of the PVDF 4–30 wt% CI blend, as well as the less uniform fiber diameter.

Incorporated CI particles are known to offer potential magnetic behavior and have previously been investigated using a VSM resulting in values between 188 and 229 emu g<sup>-1</sup> for the neat particles.<sup>[24,25]</sup> Furthermore, CI particles incorporated within a PVDF film showed a saturation magnetization commencing at 18 emu g<sup>-1</sup> for PVDF films containing 1 wt% of CI and increased with increasing particle amount to 29 emu g<sup>-1</sup> for 10 wt% as investigated by Sang et al.<sup>[5]</sup>

The magnetic behavior of the MEW-processed scaffold using the PVDF containing 30 wt% CI particles was compared to a scaffold made from neat PVDF (Video S2, Supporting Information). The scaffold containing CI particles adhered to magnets and followed its movement in contrast to the neat PVDF scaffold without particles. Furthermore, magnetic field measurements were performed for the blends containing 1, 5, 15, and 30 wt% CI particles showing magnetic activity in response to the applied field. In Videos S3 and S4 (Supporting Information), the magnetic activity of MEW scaffolds containing 1 and 30 wt% CI particles are shown with an applied magnetic field of 240 and 64 kA, respectively. All blends with CI particles showed magnetic properties and magnetoactivity increased with increasing CI particle concentration

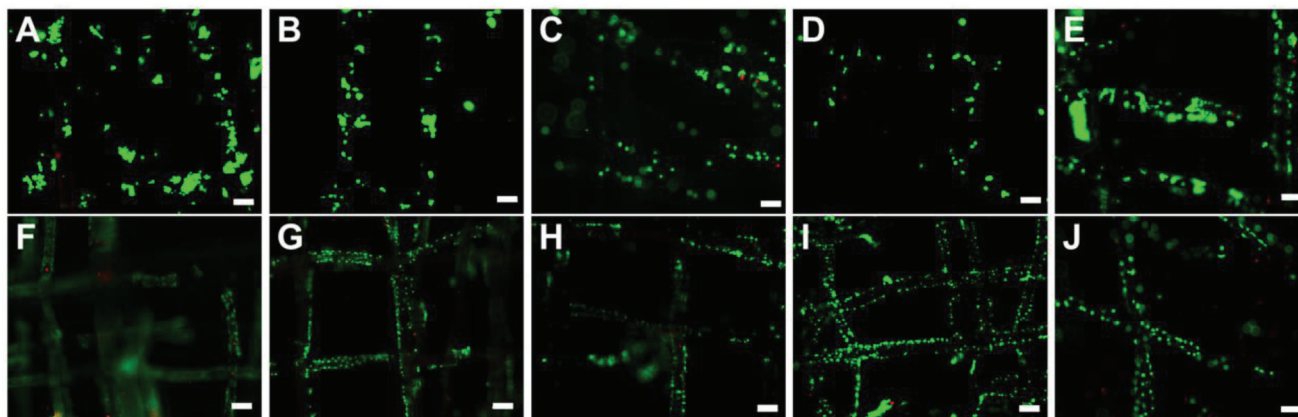


**Figure 4.** Live/Dead staining using L929 cells with the corresponding cell viability at A–E) day 1 and F–J) day 4 for MEW-processed scaffolds using A,F) neat PVDF without particles and blends containing B,G) 1 wt%, C,H) 5 wt%, D,I) 15 wt%, and E,J) 30 wt% of CI particles. Scale bars are 100  $\mu\text{m}$ . Green (Calcein AM): live cells, red (Ethidium homodimer-1): dead cells.

within the PVDF matrix. Nevertheless, further in-depth investigation of the magnetic properties might be needed depending on the chosen application.

One potential application for the magnetoactive fibers presented here is magnetically responsive 3D constructs for stimuli-responsive 4D printing. MEW allows to overcome current resolution limits of other 3D printing techniques and offers freedom in the design of scaffolds with high accuracy in fiber placement.<sup>[44]</sup> A recent study, for example, developed a MEW fiber embedded silicone tube that provided ultrafast actuation.<sup>[33]</sup> Furthermore, an improved MEW printer capable of printing more than one material at a time could further enhance the complexity of printed constructs by combining advantageous properties of different materials, such as producing shape morphing constructs<sup>[29–31,36]</sup> within a single processing step.

As a first step to expand the list of potential applications towards biomedical use, a live/dead assay was performed with L929 cells on those scaffolds at day 1 and day 4 (**Figure 4**). The cell viability at day 1 for the PVDF control was  $97 \pm 2\%$ , and  $87 \pm 8\%$ ,  $89 \pm 1\%$ ,  $82 \pm 11\%$ , and  $80 \pm 7\%$  for 1, 5, 15, and 30 wt% CI particles containing scaffolds, respectively. The fluorescence images of L929 cells on the novel hybrid materials also confirmed cells adhering well to PVDF scaffolds containing CI particles. The cell viability at day 4 was  $88 \pm 7\%$  for the neat PVDF, and  $85 \pm 8\%$ ,  $87 \pm 9\%$ ,  $87 \pm 10\%$ , and  $78 \pm 12\%$  for 1, 5, 15, and 30 wt% CI particles containing scaffolds, respectively. The lowest cell viability was shown for scaffolds containing 30 wt% CI particles. Previously, other studies also that CI particles are commonly considered as nontoxic<sup>[24,25]</sup> and, therefore, are promising candidates for biomedical applications. Nevertheless, outcomes regarding the toxicity of neat CI particles are variable,<sup>[45]</sup> and likely related to their preparation and purification.

These first cell viability test of the electroactive PVDF scaffolds containing up to 30 wt% CI particles could lead to promising applications, especially for biomechanical stimulation through loads induced via magnetic fields.<sup>[6]</sup> For such 4D printing approaches, further investigations would be needed with appropriate cells that incorporate proliferation assays, surface functionality, and mechanical stimulation. Piezoelectric PVDF containing

magnetostrictive particles such as cobalt iron oxide ( $\text{CoFe}_2\text{O}_4$ ) demonstrated promising results for bone tissue repair strategies due to the magnetomechanical and magnetoelectrical response of the material.<sup>[6]</sup> These hybrid materials have the potential for many tissue engineering applications since they can stimulate tissue regeneration via magnetic to mechanical to electrical conversion/stimuli and external scaffold control via magnetic fields.<sup>[46]</sup> Similar applications are envisioned for the presented micro periodic PVDF scaffolds.

#### 4. Conclusion

In summary, the MEW-processability of PVDF blends with up to 15 wt% CI particles provided a good balance of particle distribution, print quality, magneto-activity, and cell adhesion while avoiding nozzle clogging. Investigations of the crystalline phase using XRD and DSC showed negligible change in the material properties, and viscoelastic investigations confirmed slightly increased viscosity for the master batches with higher particles content. Furthermore, the particles did not significantly affect the printability of the blends, as we could process the melts to obtain stable jets and microfiber scaffolds. Mostly, the fabricated fibers were uniform and showed diameters between 30 and 50  $\mu\text{m}$ . Only the blend containing 30 wt% CI particles resulted in less uniform fibers, as well as less accurate placement and rougher fiber surface. Nevertheless, to the best of our knowledge, this is the highest particle amount in MEW-processed polymers without the need of additives or solvents, while still enabling a stable jet and sufficient MEW-processability without major parametric changes compared to the neat material resulting in magnetically active scaffolds even at only 1 wt% CI particle loading.

Furthermore, the cell viability of L929 cells showed similar behavior for the PVDF control sample and the blends containing up to 30 wt% CI particles with sufficient cell adherence at day 4. With further investigations into their cytocompatibility, these blends could offer potential magnetoactive cell stimulation or stimuli-responsive 4D printing using MEW. From the processing perspective, including CI particles into the melt minimally affected

the jet, offering a road map for researcher to introduce more function into MEW-processable materials.

## Supporting Information

Supporting Information is available from the Wiley Online Library or from the author.

## Acknowledgements

The authors gratefully acknowledge financial support by the Volkswagen Foundation (Grant No. 93418). In addition, J.C.K. appreciates support by the Joachim Herz Foundation and by funds of the Bavarian State Ministry of Science and the Arts and the University of Würzburg to the Graduate School of Life Sciences (GSLs), University of Würzburg, Germany. The technical assistance of Philipp Stahlhut and Judith Friedlein for SEM imaging and EDX analysis and Simon Luposchinsky for recording the magnetic properties is appreciated while the Zeiss Crossbeam CB 340 SEM was funded by the German Research Foundation (DFG) State Major Instrumentation Programme (INST 105022/58-1 FUGG). M.M. and D.G. would like to acknowledge to the Czech Science Foundation, Grant No. 19-17457S and the Ministry of Education, Youth and Sports of the Czech Republic – DKRVO (RP/CPS/2022/003) for financial support.

Open Access funding enabled and organized by Projekt DEAL.

## Conflict of Interest

The authors declare no conflict of interest.

## Data Availability Statement

The data that support the findings of this study are available from the corresponding author upon reasonable request.

## Keywords

additive manufacturing, electroactive polymers, magnetoactive materials, melt electrospinning writing

Received: July 18, 2022

Revised: August 29, 2022

Published online: September 23, 2022

- [1] C. Tsonos, H. Zois, A. Kanapitsas, N. Soin, E. Siores, G. D. Peppas, E. C. Pyrgioti, A. Sanida, S. G. Stavropoulos, G. C. Psarras, *J. Phys. Chem. Solids* **2019**, *129*, 378.
- [2] T. Prabhakaran, J. Hemalatha, *Mater. Chem. Phys.* **2013**, *137*, 781.
- [3] C. Tsonos, N. Soin, G. Tomara, B. Yang, G. C. Psarras, A. Kanapitsas, E. Siores, *RSC Adv.* **2016**, *6*, 1919.
- [4] H. Wang, Q. Fu, J. Luo, D. Zhao, L. Luo, W. Li, *Appl. Phys. Lett.* **2017**, *110*, 242902.
- [5] M. Sang, S. Wang, M. Liu, L. Bai, W. Jiang, S. Xuan, X. Gong, *Compos. Sci. Technol.* **2018**, *165*, 31.
- [6] M. M. Fernandez, D. M. Correia, C. Ribeiro, N. Castro, V. Correia, S. Lanceros-Mendez, *ACS Appl. Mater. Interfaces* **2019**, *11*, 45265.
- [7] C. Ribeiro, C. M. Costa, D. M. Correia, J. Nunes-Pereira, J. Oliveira, P. Martins, R. Gonçalves, V. F. Cardoso, S. Lanceros-Méndez, *Nat. Protoc.* **2018**, *13*, 681.
- [8] P. D. Dalton, *Curr. Opin. Biomed. Eng.* **2017**, *2*, 49.
- [9] G. Hochleitner, T. Jungst, T. D. Brown, K. Hahn, C. Moseke, F. Jakob, P. D. Dalton, J. Groll, *Biofabrication* **2015**, *7*, 035002.
- [10] T. D. Brown, P. D. Dalton, D. W. Hutmacher, *Adv. Mater.* **2011**, *23*, 5651.
- [11] J. C. Kade, P. D. Dalton, *Adv. Healthcare Mater.* **2021**, *10*, 2001232.
- [12] T. M. Robinson, D. W. Hutmacher, P. D. Dalton, *Adv. Funct. Mater.* **2019**, *29*, 1904664.
- [13] S. Vijayavenkataraman, W.-C. Yan, W. F. Lu, C.-H. Wang, J. Y. H. Fuh, *Adv Drug Delivery Rev.* **2018**, *132*, 296.
- [14] W. L. Ng, C. K. Chua, Y.-F. Shen, *Prog. Polym. Sci.* **2019**, *97*, 101145.
- [15] A. Hrynevich, P. Achenbach, T. Jungst, G. A. Brook, P. D. Dalton, *Macromol. Biosci.* **2021**, *21*, 2000439.
- [16] R. McMaster, C. Hoefner, A. Hrynevich, C. Blum, M. Wiesner, K. Wittmann, T. R. Dargaville, P. Bauer-Kreisel, J. Groll, P. D. Dalton, T. Bunk, *Adv. Healthcare Mater.* **2019**, *8*, 1801326.
- [17] N. Fischhaber, J. Faber, E. Bakirci, P. D. Dalton, S. Budday, C. Villmann, N. Schaefer, *Adv. Healthcare Mater.* **2021**, *10*, 2100830.
- [18] S. Florczak, T. Lorson, T. Zheng, M. Mrlik, D. W. Hutmacher, M. J. Higgins, R. Luxenhofer, P. D. Dalton, *Polym. Int.* **2019**, *68*, 735.
- [19] J. C. Kade, P. F. Otto, R. Luxenhofer, P. D. Dalton, *Polym. Adv. Technol.* **2021**, *32*, 4951.
- [20] A. Abdal-Hay, N. Abbasi, M. Gwiazda, S. Hamlet, S. Ivanovski, *Eur. Polym. J.* **2018**, *105*, 257.
- [21] N. C. Paxton, J. Ren, M. J. Ainsworth, A. K. Solanki, J. R. Jones, M. C. Allenby, M. M. Stevens, M. A. Woodruff, *Macromol. Rapid Commun.* **2019**, *40*, 1900019.
- [22] E. Hewitt, S. Mros, M. Mcconnell, J. Cabral, A. Ali, *Biomed. Mater.* **2019**, *14*, 055013.
- [23] K. Somszor, O. Bas, F. Karimi, T. Shabab, N. T. Saïdy, A. J. O'Connor, A. V. Ellis, D. Hutmacher, D. E. Heath, *ACS Macro Lett.* **2020**, *9*, 1732.
- [24] M. Cvek, M. Mrlik, M. Ilčíková, J. Mosnáček, V. Babayan, Z. Kuceková, P. Humpolíček, V. Pavlínek, *RSC Adv.* **2015**, *5*, 72816.
- [25] M. Mrlik, M. Ilčíková, M. Cvek, V. Pavlínek, A. Zahoranová, Z. Konečková, P. Kasak, *RSC Adv.* **2016**, *6*, 32823.
- [26] D. Min, W. Zhou, F. Luo, D. Zhu, *J. Magn. Magn. Mater.* **2017**, *435*, 26.
- [27] Y. Qing, D. Min, Y. Zhou, F. Luo, W. Zhou, *Carbon* **2015**, *86*, 98.
- [28] D. Nahm, *PhD Thesis Poly(2-oxazine) Based Biomaterial Inks for Additive Manufacturing of Microperiodic Hydrogel Scaffolds*, University of Würzburg, **2021**. <https://doi.org/10.25972/OPUS-24598>
- [29] G. Constante, I. Apsite, H. Alkhamis, M. Dulle, M. Schwarzer, A. Caspari, A. Synytska, S. Salehi, L. Ionov, *ACS Appl. Mater. Interfaces* **2021**, *13*, 12767.
- [30] J. Uribe-Gomez, A. Posada-Murcia, A. Shukla, M. Ergin, G. Constante, I. Apsite, D. Martin, M. Schwarzer, A. Caspari, A. Synytska, S. Salehi, L. Ionov, *ACS Appl. Bio Mater.* **2021**, *4*, 1720.
- [31] A. Kirillova, R. Maxson, G. Stoychev, C. T. Gomillion, L. Ionov, *Adv. Mater.* **2017**, *29*, 1703443.
- [32] X. Kuang, D. J. Roach, J. Wu, C. M. Hamel, Z. Ding, T. Wang, M. L. Dunn, H. J. Qi, *Adv. Funct. Mater.* **2019**, *29*, 1805290.
- [33] O. Bas, B. Gorissen, S. Luposchinsky, T. Shabab, K. Bertoldi, D. W. Hutmacher, *Multifunct. Mater.* **2021**, *4*, 045001.
- [34] A. Y. Chen, E. Pegg, A. Chen, Z. Jin, G. X. Gu, *Adv. Intell. Syst.* **2021**, *3*, 2100019.
- [35] P. Zhu, W. Yang, R. Wang, S. Gao, B. Li, Q. Li, *ACS Appl. Mater. Interfaces* **2018**, *10*, 36435.
- [36] W. Zhao, F. Zhang, J. Leng, Y. Liu, *Compos. Sci. Technol.* **2019**, *184*, 107866.
- [37] Y. Zhang, Q. Wang, S. Yi, Z. Lin, C. Wang, Z. Chen, L. Jiang, *ACS Appl. Mater. Interfaces* **2021**, *13*, 4174.

- [38] M. M. Chamakh, M. Mrlík, S. Leadenham, P. Bažant, J. Osička, M. A. A. AlMaadeed, A. Erturk, I. Kuřitka, *Nanomaterials* **2020**, *10*, 2345.
- [39] W. Ma, J. Zhang, X. Wang, S. Wang, *Appl. Surf. Sci.* **2007**, *253*, 8377.
- [40] C. Bohm, P. Stahlhut, J. Weichhold, A. Hrynevich, J. Tessmar, P. D. Dalton, *Small* **2022**, *18*, 2104193.
- [41] M. Mrlík, J. Osička, M. Cvek, M. Ilčíková, P. Srnec, D. Gorgol, P. Tofel, *Nanomaterials* **2021**, *11*, 1637.
- [42] J. C. Kade, B. Tandon, J. Weichhold, D. Pisignano, L. Persano, R. Luxenhofer, P. D. Dalton, *Polym. Int.* **2021**, *70*, 1725.
- [43] D.-C. Silveira, T.-T. da Silva Braga<sup>1</sup>, D.-M. Gil, N. Adriano, dos Santos Gomes, L.-M. Guerrini, E.-C. Botelho, *J. Renewable Mater.* **2019**, *7*, 279.
- [44] I. Liashenko, A. Hrynevich, P. D. Dalton, *Adv. Mater.* **2020**, *32*, 2001874.
- [45] V. Valdíglesias, G. Kiliç, C. Costa, N. Fernández-Bertólez, E. Pásaro, J. P. Teixeira, B. Laffon, *Environ. Mol. Mutagen.* **2015**, *56*, 125.
- [46] B. Hermenegildo, C. Ribeiro, L. Pérez-Álvarez, J. L. Vilas, D. A. Learmonth, R. A. Sousa, P. Martins, S. Lanceros-Méndez, *Colloids Surf., B* **2019**, *181*, 1041.